Computational and Structural Biotechnology Journal 21 (2023) 4944–4959

Contents lists available at ScienceDirect

Computational and Structural Biotechnology Journal

journal homepage: www.elsevier.com/locate/csbj

Research article

Development and validation of a novel DNA damage repair-related long non-coding RNA signature in predicting prognosis, immunity, and drug sensitivity in uterine corpus endometrial carcinoma

Tao Wang, Mei Ji, Wenwen Liu, Jing Sun *

Department of Gynecology, Shanghai Key Laboratory of Maternal-Fetal Medicine, Shanghai Institute of Maternal-Fetal Medicine and Gynecologic Oncology, Shanghai First Maternity and Infant Hospital, School of Medicine, Tongji University, Shanghai 200092, China

ARTICLE INFO

Keywords:
DNA damage repair
Long non-coding RNAs
Precise medicine
Prognosis
Tumor microenvironment
Uterine corpus endometrial carcinoma

ABSTRACT

Background: DNA damage response (DDR) confer resistance to chemoradiotherapy in cancer cells. However, the role of DDR-related lncRNAs (DRLs) in uterine corpus endometrial carcinoma (UCEC) is poorly understood. In this study, we aimed to identify a DRL-related prognostic signature that could guide the clinical treatment of UCEC.

Methods: We extracted transcriptome and clinical data of patients with UCEC from The Cancer Genome Atlas (TCGA) database and identified DRLs using Spearman correlation analysis. Univariate and multivariate Cox analyses were used to determine candidate prognostic DRLs. The samples were randomly divided into training and test cohorts in a 1:1 ratio. A DRL-related risk signature was constructed from the training cohort data using the least absolute shrinkage and selection operator (LASSO) algorithm, and validated using the test and entire cohorts. Subsequently, a prognostic nomogram was developed using a multivariate Cox regression analysis. The functional annotation, immune microenvironment, tumor mutation burden (TMB), immune checkpoint blockade (ICB) efficacy, and drug sensitivity were also comprehensively analyzed between different risk groups. Finally, the function of AC019069.1 was validated in vitro.

Results: A novel risk signature was developed based on nine DRLs. The risk score efficiently predicted the prognosis of patients with UCEC. Based on the median risk score, two subgroups were identified. The DDR-related pathways were upregulated in the high-risk group. Additionally, high-risk patients have low immune activity, poor response to ICB, and weak sensitivity to chemotherapeutic agents, possibly because of the proficient DDR system. Finally, we demonstrated AC019069.1 could promote cell proliferation, decrease apoptosis and maintain genome stability of UCEC cells.

Conclusions: The developed DRL-related signature can predict the prognosis, immune microenvironment, immunotherapy, and chemoradiotherapy responsiveness of UCEC. Our study also revealed the potential value of DDR-targeted therapy in treating high-risk patients with UCEC.

1. Introduction

Uterine corpus endometrial carcinoma (UCEC) is the fourth most common malignancy in females worldwide, with an increasing incidence and cancer-associated mortality [1]. Generally, UCEC prognosis is satisfactory at the early stage, with approximately 81% 5-year overall

Abbreviations: UCEC, Uterine corpus endometrial carcinoma; DDR, DNA damage repair; LncRNAs, Long noncoding RNAs; TCGA, The Cancer Genome Atlas; DRGs, DDR-related genes; DRLs, DDR-related lncRNAs; DElncRNAs, Differentially expressed lncRNAs; DEDRLs, Differentially expressed DRLs; LASSO, Least absolute shrinkage and selection operator; ROC, Receiver operator characteristic; DEGs, Differentially expressed genes; GO, Gene ontology; KEGG, Kyoto Encyclopedia of Genes and Genomes; GSEA, Gene Set Enrichment Analysis; ssGSEA, single-sample GSEA; ESTIMATE, Estimation of Stromal and Immune cells in Malignant Tumor tissues using Expression data; IPS, Immunophenoscore; TCIA, The Cancer Immunome Atlas; ICB, Immune checkpoint blockade; TIDE, Tumor Immune Dysfunction and Exclusion; TMB, Tumor burden mutation; MSI, Microsatellite instability; MSS, Microsatellite stability; GDSC, Genomics of Drug Sensitivity in Cancer; IC50, Half-maximal inhibitory concentration.

* Corresponding author.
E-mail address: sunjing61867@tongji.edu.cn (J. Sun).

https://doi.org/10.1016/j.csbj.2023.10.025
Received 24 July 2023; Received in revised form 13 October 2023; Accepted 13 October 2023
Available online 14 October 2023

survival (OS) rate. However, when diagnosed at a late stage, the 5-year OS rate declines to < 20% [2]. Although divergent therapeutic regimens have been developed to improve UCEC prognosis, the clinical management of this complex disease remains challenging owing to its high degree of heterogeneity. Typically, this disease is classified as type I (estrogen-driven with favorable prognosis) or type II (estrogen-independent with unfavorable outcome) [3]; however, the prognosis of patients with the same type varies greatly. Recently, molecular subtyping has been proposed as a precise method for guiding cancer management. Therefore, novel molecular classification systems incorporating genetic diversity should be urgently developed to accurately predict UCEC prognosis and therapeutic response, which are crucial for the optimal design of next-generation precision medicine.

Uncontrolled cell proliferation associated with substantial DNA damage accumulation and genomic instability causes tumorigenesis. Efficient DNA damage repair (DDR) mechanisms are essential for maintaining genomic integrity and preventing cancer development [4]. However, in addition to the barrier role of DDR in tumor initiation, proficient DDR can also confer resistance to tumor therapy. Radiotherapy and chemotherapy are two cornerstones of cancer management. Theoretically, they partially kill tumor cells by triggering DNA breaks [5]. Evidently, the activation of DDR could help cancer cells escape from such treatment. Additionally, DDR plays considerable roles in UCEC. Fanconi anemia complementation group D2 (FANCD2), a core component of the Fanconi anemia repair pathway, is overexpressed in UCEC and predicts poor OS. FANCD2 expression knockdown in UCEC cell lines sensitizes UCEC cells to cisplatin and mitomycin C [6]. Furthermore, the inhibitors of ataxia telangiectasia-mutated (ATM) and ATR (ATM and Rad3-related), two critical DDR molecules, boost the sensitivity of UCEC cells to common DNA-damaging agents [7]. Thus, targeting the DDR pathways could be a promising therapy for UCEC.

Long non-coding RNAs (lncRNAs) are > 200 nucleotide long non-coding transcripts that act as crucial and precise regulators of cancer development and progression [8,9]. Previous studies have revealed that lncRNAs are dysregulated and play diverse roles in the carcinogenesis, metastasis, and therapeutic resistance of UCEC [10]. Several lncRNA-related prognostic models have been developed to aid the clinical management of UCEC [11–13]. Nevertheless, the role of DDR-related lncRNAs (DRLs) in UCEC has not been comprehensively explored.

In this study, we extracted transcriptome profiles and clinical data from The Cancer Genome Atlas (TCGA) database to identify candidate DRLs and construct a related prognostic signature. Through comprehensive bioinformatics analyses, a promising DDR-related differentially expressed lncRNA-based signature was constructed, which could predict the outcomes of patients with UCEC and provide a theoretical basis for selecting patients for reasonable therapies. Moreover, we tentatively confirmed the role of AC019069.1 in regulating the DDR in UCEC.

2. Materials and methods

2.1. Data acquisition and processing

The transcriptome profiles (count format) of 548 UCEC samples and 35 control tissues, and the clinical data of patients with UCEC were obtained from The Cancer Genome Atlas (TCGA) database (https://xena.ucsc.edu/), and only genes expressed in more than 50% samples were analyzed. The raw count data were normalized using "cpm" function in the R package "edgeR" and $\log_2$ (cpm+1) transformed, except for the analysis of differentially expressed genes (DEGs). For risk model construction and validation, only 521 unique tumor samples with complete survival data, at least 30 days of survival period were included. Then, they were randomly separated into the training cohort (261 cases) and the test cohort (260 cases) using the "caret" R package (seed:12345); the clinical characteristics of patients with UCEC in the training and test cohorts were summarized in Table S1. The training cohort was used for risk model construction, whereas the test and entire cohorts were used for validation.

2.2. DDR-related lncRNA identification

The DDR-related lncRNAs (DRLs) were identified from lncRNAs and 296 DDR-related genes (DRGs) identified previously [14] (Table S2) using Spearman's correlation ($|r| > 0.4$ and $P < 0.001$). Then, the "limma" package [15] was utilized to screen the DElncRNAs between tumor and normal samples. The criteria for DElncRNAs were $|\text{fold change}| > 2$ and adjusted $P < 0.05$. The intersecting regions of the DRLs and DElncRNAs were defined as differentially expressed DRLs (DEDRLs).

2.3. Consensus clustering

Tumors can be divided into diverse subtypes based on their omics profiles. We used consensus clustering to assess the heterogeneity of UCEC based on DEDRL expression data using "partitioning around medoids" method on the "ConsensusClusterPlus" package [16]. To ensure stable subtype classification, the parameter "reps" was set to 500.

2.4. DEDRL-related prognostic model construction and validation

First, univariate Cox regression was applied to acquire OS-related DEDRLs ($P < 0.05$); then, the genes were re-filtered through multivariate Cox regression analysis according to "forward and backward" method to identify candidate independent prognostic DEDRLs. Subsequently, the least absolute shrinkage and selection operator (LASSO) Cox regression algorithm was used to develop an optimal risk model based on these prognostic candidates in the training cohort. Finally, a nine-DEDRL-based optimal prognostic model was established by selecting the optimal penalty parameter (λ). LASSO algorithm was conducted with the "glmnet" R package. The risk score was determined as

$$\text{risk score} = \sum_{1}^{n} \text{coefi} \times \text{DEDRLi},$$

where DEDRLi and coefi denote the expression of the selected lncRNAs and their corresponding coefficients, respectively. And n refers to the number of DEDRLs considered in the constructed model.

Based on the median risk score in each cohort, the samples were divided into low- and high-risk subgroups. A flowchart to explain the development of the prognostic model was shown in Fig. S1. Kaplan–Meier curves were drawn using the "survival" package to compare OS between the two groups. The receiver operator characteristic (ROC) curves were drawn via the "timeROC" package to evaluate the 1-, 3-, 5-year predictive accuracy of the signature.

2.5. Establishment of prognosis nomogram in combination with clinical characteristics

The nomogram was established by combining the risk score and other clinical features (age, stage, and grade) to guide the clinical practice using the "rms" package. The decision curve analysis (DCA) and calibration curves were used to assess the net clinical benefit and predictive accuracy of the nomogram, respectively.

2.6. Functional enrichment analysis

To investigate potential molecular and biological differences between low- and high-risk subgroups, DEGs were identified. Then, gene set enrichment analysis (GSEA) was used to identify the enriched pathways (q-value < 0.05, FDR < 0.25) in these two subgroups based on the KEGG gene sets. In addition, single-sample GSEA (ssGSEA) was conducted to determine the relative pathway score for classical DDR-

related pathways, X-ray and UV Response using the "GSVA" R package.

2.7. Immune microenvironment exploration and immunotherapy response prediction

The abundance of 28 immune cell types and scores of 13 immune-related pathways in each sample were calculated using ssGSEA. The Estimation of STromal and Immune cells in Malignant Tumor tissues using Expression data (ESTIMATE) algorithm was conducted to acquire the content of stromal and immune elements by the "estimate" R package [17]. The immunophenoscore (IPS) is used to quantify individual patient immunogenicity. IPSs were obtained from The Cancer Immunome Atlas (TCIA) database (https://tcia.at/home) [18]. The responses of patients with UCEC to immune checkpoint blockade (ICB) were also predicted using the Tumor Immune Dysfunction and Exclusion (TIDE) algorithm, where high TIDE scores represent poor therapeutic response [19].

2.8. Mutation analysis and chemotherapy response

Simple nucleotide variation profiles of patients were acquired from TCGA. The top 10 mutated genes in low- and high-risk subgroups were presented with fall plots using the "maftools" package [20]. We also analyzed the differences in TMB. Microsatellite instability (MSI) is a specific genomic instability characterized by mutational alterations in simple repetitive sequences [21]. MSI scores were calculated with the R package "cBioPortalData." Patients with UCEC were separated into MSI and microsatellite stability (MSS) groups using a cutoff value of 0.4 and their response to therapeutic agents were predicted using the Genomics of Drug Sensitivity in Cancer (GDSC) database (https://www.cancerrxgene.org). Therapeutic sensitivity was quantified using the half-maximal inhibitory concentration (IC50). The Spearman correlation algorithm was used to quantify the relationship between the risk score and drug sensitivity.

2.9. Tissue specimens

Tissues were obtained from 19 patients with endometrial cancer (EC) who underwent surgery at Shanghai First Maternity and Infant Hospital between 2018 and 2022. This study was approved by the Medical Ethics Committee of Shanghai First Maternity and Infant Hospital (KS22356), and written informed consent was obtained from all participants.

2.10. Cell culture and cell transfection

Ishikawa, HEC-1B, and ANC3A endometrial cancer cell lines were purchased from American Type Culture Collection (ATCC, USA) and cultured in Dulbecco's modified Eagle's medium (DMEM)-F12 (Servicebio, Wuhan, China) supplemented with 10% fetal bovine serum (0500, Sciencell, USA) and 1% penicillin/streptomycin (C100C5, NCM, Suzhou, China) at 37 °C with 5% CO_2 supply. The cells were treated with 20 μM etoposide (MedChemExpress, USA) for 2 h to induce DNA damage and harvested (damage induction) or cultured in fresh medium for 4 h (damage recovery). The AC019069.1-overexpression plasmid was purchased from Genomeditech (Shanghai, China). At 50–60% confluence, cells were transfected with Lipofectamine 2000 (Invitrogen, USA).

2.11. RNA extraction and quantitative real-time PCR (qRT-PCR)

The TRIzol reagent (ABclonal, Wuhan, China) was used for total RNA isolation. Then, 1 μg RNA was reversely transcribed into cDNA. Quantitative PCR was conducted using QuantStudio5 (Thermo Fisher Scientific, Waltham, USA) for 40 cycles. The relative expression of interested genes was determined with $2^{-\Delta\Delta CT}$ algorithm with β-actin as a reference control. The primers used in this study are listed in Table S3.

2.12. Western blot

First, EC cells were transfected with empty vector or AC019069.1-overexpression plasmid for 48 h. Then cells were collected after treatment with etoposide (20 μM) for the indicated time. A radioimmunoprecipitation (RIPA) buffer (EpiZyme, Shanghai, China) containing 1% protease inhibitors (NCM; Suzhou, China) was used for protein lysis and extraction. Then, 15 μg proteins were separated on a 12.5% sodium dodecyl sulfate (SDS) polyacrylamide gel and then transferred to a 0.45 μm polyvinylidene fluoride membrane (IPVH00010, Millipore, German). After being blocked in 5% non-fat milk for 1 h, the membranes were incubated with the following antibodies at 4 °C overnight: phospho-Histone H2A.X (Ser139) (γH2AX; #9718, Cell Signaling Technology, USA), GAPDH (ab181602, Abcam, USA), Histone H3 (A2348, ABclonal, Wuhan, China). Histone 3 was used as an internal control for histone. GAPDH was used as a reference control for total protein. Next, the membranes were incubated with a secondary antibody (GB23204, Servicebio, Wuhan, China) at room temperature for 1 h. Finally, protein bands of interest were visualized using a Tanon exposure machine and further quantified using ImageJ software.

2.13. Counting Kit-8 (CCK-8) assay

CCK-8 reagent (NCM, Suzhou, China) was used to monitor cell proliferation according to the manufacturer's instructions. Briefly, 2×10^3 cells/well were seeded in 96-well plates and cultured for 0, 24, 48, 72, or 96 h. Then, 10 μL CCK-8 reagent was added to the medium and cultured at 37 °C for another 2 h. Finally, the absorbance at 450 nm was quantified on a microplate reader.

2.14. 5-ethynyl-20-deoxyuridine (EdU) assay

EdU Cell Proliferation Kit was purchased from Epizyme (CX003, Shanghai, China). Briefly, 1×10^5 transfected cells/well were seeded into 12-well plates. EdU solution (final concentration: 10 μM) was added to the medium when the cells adhered, and another 2 h were incubated. After fixing and permeabilization, a click additive solution was added and incubated in dark for 30 min. The cells were then counterstained with Hoechst 33342. EdU-incorporated cells were visualized using a Leica fluorescence microscope (Wetzlar, Germany) and counted using ImageJ software.

2.15. Apoptosis

First, the transfected EC cells were digested and collected using trypsin without EDTA. The cells were then incubated with Annexin V–FITC and PI (40302ES50, Yeasen, Shanghai, China) for 25 min. Cell apoptosis rates were determined using flow cytometry.

2.16. Immunofluorescence

The transfected EC cells (5×10^4 cells/well) were seeded on sterile coverslips in 12-well plates. After the indicated treatments, cells were fixed, permeabilized, and blocked. Then, the cells were incubated with γH2AX antibody (1:500) overnight at 4 °C and fluorescent secondary antibody (1:200; ab150077, Abcam, USA) in dark for 1 h. Afterward, the cells were mounted with anti-fluorescence quenching mounting solution (containing DAPI) (Beyotime, Shanghai, China) and imaged under Leica confocal microscope (Wetzlar, Germany).

2.17. Statistical analysis

All statistical analyses were performed using R software (version 4.1.1). For continuous variables, Student's *t*-test (two groups) or one-way ANOVA (over two groups) was applied to assess intergroup

differences when the data followed a normal distribution; otherwise, the Wilcoxon rank-sum test (two groups) or Kruskal-Wallis H test (over two groups) was used. For categorical variables, χ^2 test was applied to estimate the differences among groups. All statistical analyses were two-sided and $P < 0.05$ indicated statistically significant.

3. Results

3.1. DEDRL identification in UCEC

The research diagram is shown in Fig. 1. To preliminarily examine the role of DDR in UCEC, we performed GSEA and ssGSEA on the 296 collected DRGs. The GSEA results indicated that the pre-defined DDR gene set was positively enriched in UCEC samples (q-value < 0.001; Fig. 2A). Similarly, the DDR score calculated using ssGSEA was higher in the UCEC samples than that in control samples (Fig. 2B), suggesting that DDR might participate in UCEC progression.

Considering the regulatory roles of lncRNAs, we screened DRLs in the TCGA-UCEC project. In total, 6174 lncRNAs were identified in tumor samples and in control samples. Consequently, 751 DRLs were identified using the Spearman's correlation algorithm. We identified 1670 DElncRNAs between tumor and control samples, including 964 downregulated and 706 upregulated lncRNAs. Finally, 204 DEDRLs were identified by intersecting the DRLs and DElncRNAs (Fig. 2C).

3.2. UCEC subtype classification based on the DEDRLs

To explore the heterogeneity of UCEC based on DEDRLs, a consensus clustering algorithm was applied to the TCGA-UCEC tumor samples. The optimal cluster parameter was chosen as K= 2 (Fig. 2D and S2). The tumor samples were separated into two subgroups based on the clustering results. The PCA plot revealed significantly distinct DEDRL expression patterns between the two clusters (Fig. 2E). Moreover, cluster2 had a significantly shorter OS than cluster1 (Fig. 2F).

To further investigate the potential mechanisms underlying the prognostic heterogeneity, we comprehensively analyzed the immune microenvironments of these two clusters. First, we found most immune cell types showed less infiltrated in cluster2 (Fig. S3A). In addition, the stromal, immune, and estimated scores in cluster2 were significantly lower than those in cluster1 (Fig. S3B). Most 13 immune-related pathways were enriched in cluster1 (Fig. S3C). These findings indicate that the reduced immune activity of cluster2 may favor tumor progression. Furthermore, most of the 35 validated checkpoints were downregulated in cluster2 group (Fig. S3D), which might suggest weak ICB sensitivity. The IPS and TIDE (Fig. 3E, F) analyses revealed a poorer ICB response in cluster2 group. Altogether, DEDRLs may aid in novel UCEC subtype stratification and prediction of immunotherapy efficacy.

3.3. Development and validation of a DEDRL prognostic model

Furthermore, we determined the prognostic value of DEDRLs. Totally, twelve candidate prognostic DEDRLs were screened (Fig. 2G). The correlation between these 12 lncRNAs and their corresponding DRGs was visualized using a heat map (Fig. 2H). Then, the LASSO algorithm was employed to prevent overfitting by choosing "lambda.min" as the optimal penalty parameter in the training cohort (Fig. 3A, B). Finally, a nine-DEDRL-based signature was constructed, and their relative expression levels were studied using a volcano plot (Fig. 3C). Each

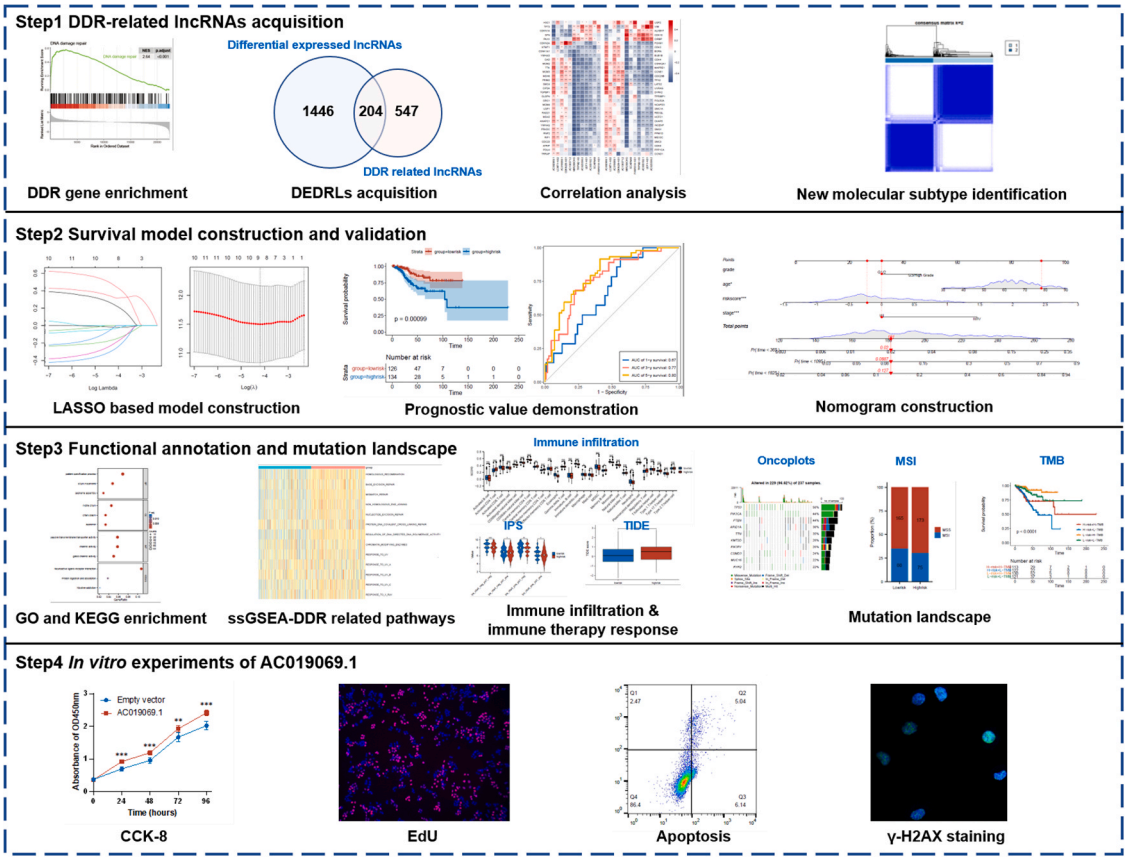

Fig. 1. Workflow and result summary of this study. **Step1.** The identification of differentially expressed DNA damage repair-related lncRNAs (DEDRLs) in uterine corpus endometrial carcinoma (UCEC). **Step2.** The construction and validation of a DEDRL-related prognostic model based on LASSO algorithm. **Step3.** The comprehensive comparisons of molecular characteristics, immune microenvironment, tumor mutation burden (TMB), immune checkpoint blockade (ICB) efficacy, and drug sensitivity between the low- and high-risk groups. **Step4.** *In vitro* experiments were conducted to reveal the function of AC019069.1 in UCEC.

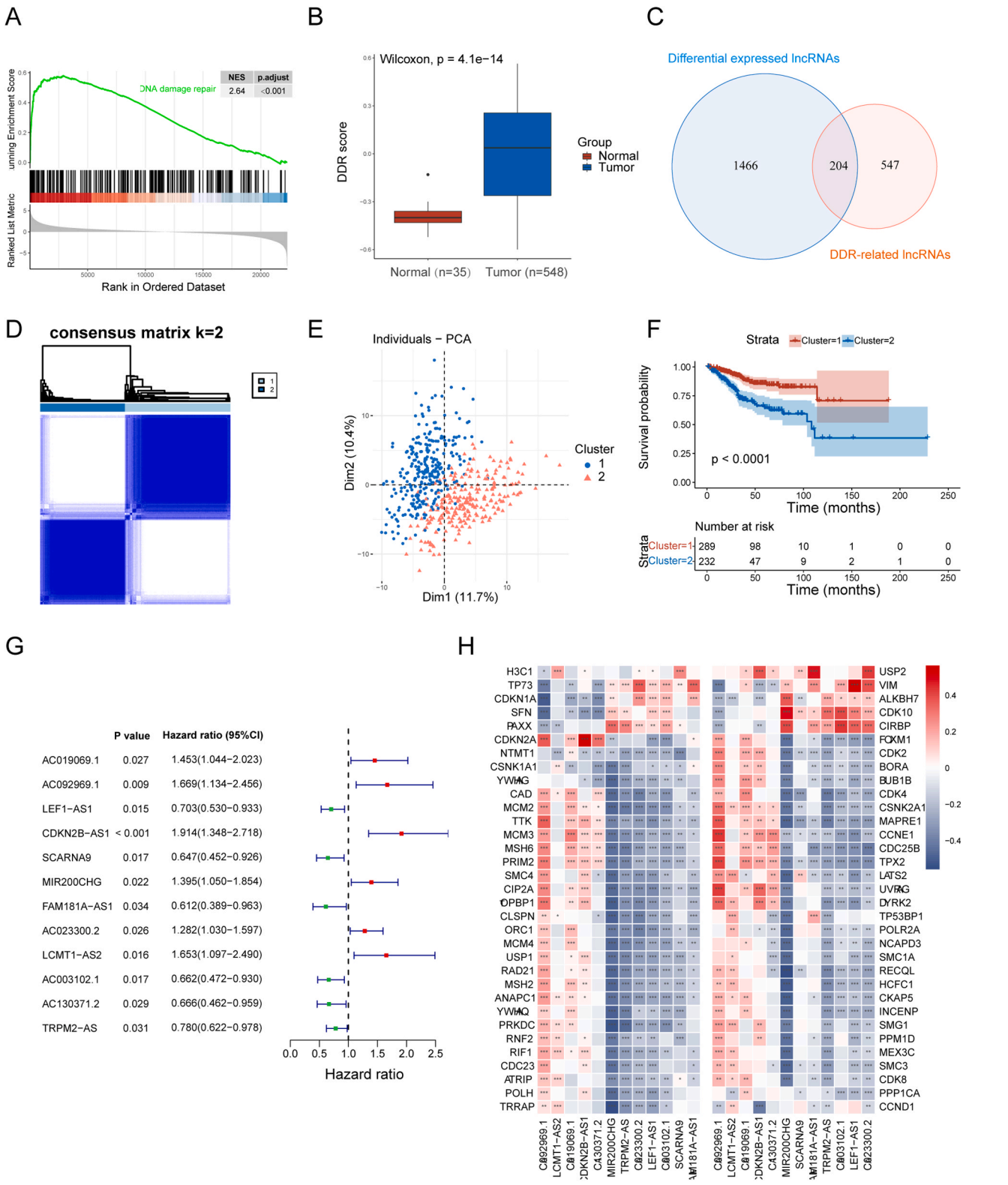

Fig. 2. A screen of candidate prognostic DNA damage repair (DDR)-related lncRNAs in uterine corpus endometrial carcinoma (UCEC). (A) The gene set enrichment analysis (GSEA) showing the positive enrichment of DDR in tumor samples. NES, normalized enrichment score. (B) The relative DDR scores calculated using single sample GSEA (ssGSEA) algorithm between normal and tumor samples. (C) Venn diagram to identify differentially expressed DDR-related lncRNAs (DEDRLs) in UCEC. (D) The consensus score matrix for K = 2. (E) Principal component analysis (PCA) based on the expression levels of DEDRLs. (F) Kaplan–Meier analysis for the two clusters in UCEC. (G) Forest plots showing the prognostic value of 12 candidate DEDRLs. (H) The correlation between 12 candidate prognostic DEDRLs and the corresponding DDR genes in the TCGA-UCEC cohort. Spearman correlation analysis was applied. The color of each table cell represents the degree of relationship. *p < 0.05, * *p < 0.01, and * **p < 0.001.

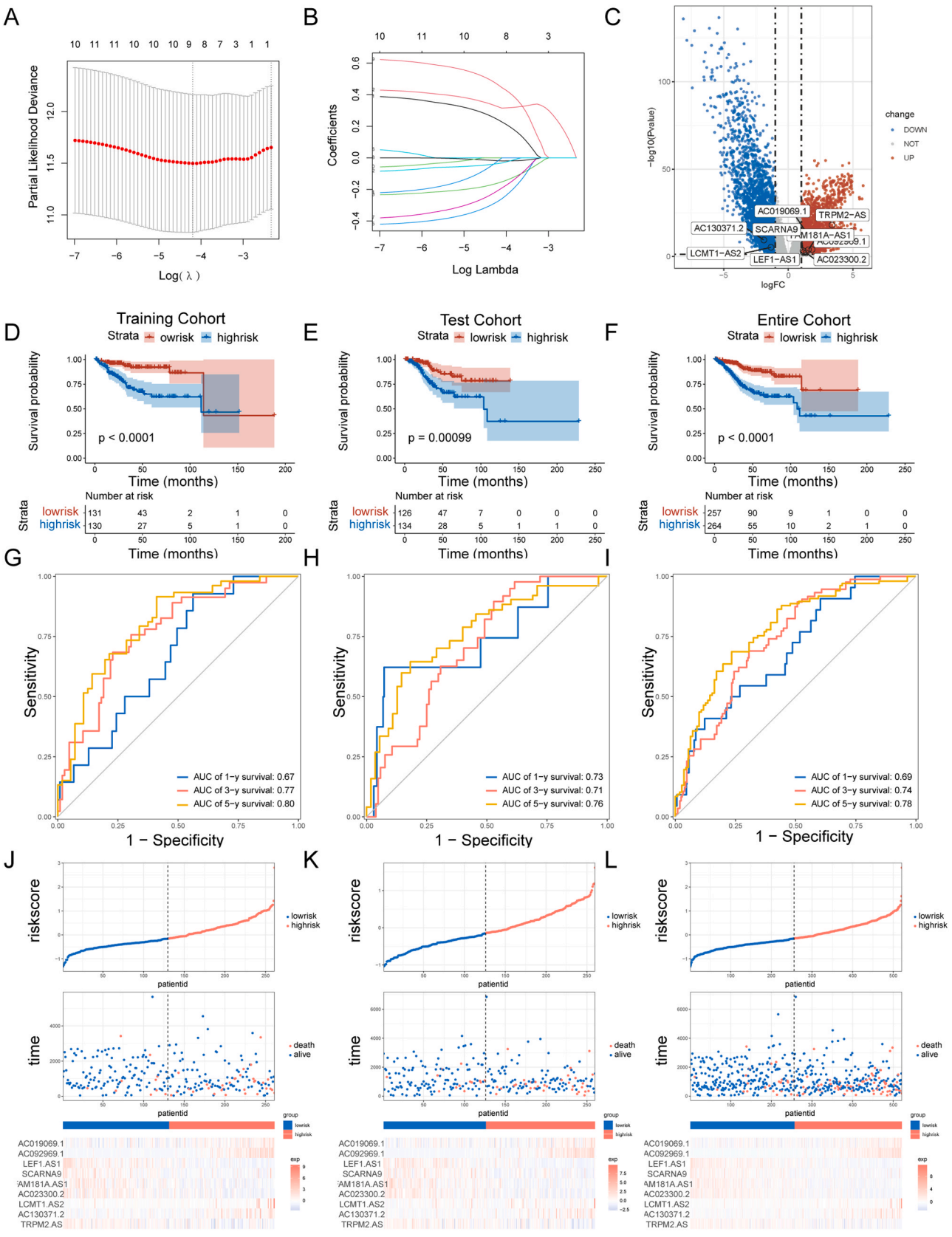

Fig. 3. Identification of a prognosis model based on a nine-DEDRL signature. (A, B) LASSO Cox regression with minimum lambda as the optimal parameter identifying the prognostic DEDRLs. (C) Volcano plot depicting the expression levels of the nine signature lncRNAs between the normal and tumor groups. Red denotes upregulated genes while blue denotes downregulated genes. (D-F) Kaplan–Meier analysis of risk score for training (D), test (E), entire (F) TCGA-UCEC cohorts. (G-I) The time-dependent receiver operating characteristic (ROC) analyzes assessing the prognostic predictive ability of the risk signature in the training (G), test (H), and entire (I) cohorts. (J-L) Distribution of risk score, overall survival status of each UCEC patient, and the expression heatmap of the nine prognostic lncRNAs in the (J) training, (K) test, and entire (L) cohorts.

patient with UCEC was assigned a risk score utilizing the following equation:

$$\begin{aligned}\text{risk score} = {} & (\text{AC019069.1} \times 0.242) + (\text{AC092969.1} \times 0.324) + (\text{LEF1} - \text{AS1} \\ & \times (-0.160)) + (\text{SCARNA} \times (-0.275)) + (\text{FAM181A} - \text{AS1} \\ & \times (-0.207)) + (\text{AC023300.2} \\ & \times (-0.018)) + (\text{LCMT1} - \text{AS2} \times 0.463) + (\text{AC130371.2} \\ & \times (-0.019)) + (\text{TRPM2} - \text{AS} \times (-0.036))\end{aligned}$$

Subsequently, the UCEC samples were divided into low- and high-risk groups based on the median risk score. In the training cohort, the KM curves revealed that the high-risk group had a shorter OS than the low-risk group ($P < 0.0001$; Fig. 3D). The area under the curve (AUC) values for the 1-, 3-, and 5-year survival rates were 0.67, 0.77, and 0.80, respectively (Fig. 3G). The efficacy of the risk model was further confirmed in the test (Fig. 3E, H) and entire (Fig. 3F, I) UCEC cohorts. The cutoff values in these two validation cohorts were the corresponding median risk scores. The distribution of survival period and status for each individual and the expression patterns of the nine lncRNAs in the three cohorts are shown in Fig. 3J-L. Together, these data suggest that our nine-lncRNA signature can accurately predict the prognosis of patients with UCEC.

3.4. Relationship between the nine-DEDRL signature and the clinicopathological features

We then evaluated whether the risk scores varied among subgroups with different clinicopathological features. We found that high UCEC grade implied high risk scores (Fig. 4A). The same trend was observed for stage (Fig. 4B). In addition, the older (age > 60 years) subgroup also had high risk scores ($P < 0.0001$; Fig. 4C), and we also graphed a histogram to reveal the change trend of risk scores along with the age of individuals (Fig. S4). We compared the differences between the two DEDRL-based heterogeneous clusters. Cluster1 had lower risk scores compared to cluster2 ($P < 0.0001$; Fig. 4D). A Sankey diagram was drawn to depict the relationships among cluster, risk score, and patient survival status. As shown, a high proportion of patients in the cluster1 belonged to the low-risk group, and a low proportion of patients in the low-risk group died during the follow-up period (Fig. 4E). The differences in clinicopathological features between the low- and high-risk groups are displayed using a heatmap, which further showed the relative expression levels of nine signature genes between the low- and high-risk groups, and revealed that the low-risk group contained more low-stage, low-grade, young and cluster1 cases (Fig. 4F). In summary, these results suggest that our nine-DEDRL signature is closely correlated with the classical clinicopathological characteristics.

3.5. Development of a prognosis nomogram

To investigate whether the nine-DEDRL signature could independently affect UCEC prognosis, univariate and multivariate Cox regression analyses were performed by combining the risk scores with other traditional clinical features. The risk score was identified as an independent prognostic factor for UCEC (Fig. 5A, B). A nomogram incorporating risk score and other traditional clinical characteristics was then constructed to guide clinical practice. The prognostic nomogram predicted the survival probability of patients by adding the scores for the relevant factors. Specifically, the total score for a given patient was 181 (indicated by red dots and line segments), and the probabilities of 1-year, 3-year and 5-year survival for score 181 were 0.98, 0.911, and 0.873, respectively (Fig. 5C). The AUC values for 1-, 3-, and 5-year survival for the nomogram model were 0.79, 0.78, and 0.81, respectively, overwhelming any of the other indicators (Fig. 5D-F). The nomogram model has the highest net benefit for 1-, 3-, and 5-year OS, as revealed by DCA analysis (Fig. S5A). Meanwhile, the calibration curves for 1-, 3-, and 5-year OS were exactly coincident with the 45° line (Fig. S5B), implying an excellent performance. Therefore, the prognostic nomogram may potentially assist in clinical practice.

3.6. Functional enrichment of the nine-DEDRL signature

To further explore the potential mechanisms underlying the prognostic heterogeneity in these two risk groups, we performed GSEA analysis of the DEGs between these two risk subgroups in TCGA-UCEC. First, 1629 DEGs were identified, including 941 downregulated and 688 upregulated genes. The top five pathways enriched in the high- (Fig. 6A) and low-risk (Fig. 6B) groups, revealed by GSEA, were identified. As shown, the cell cycle and DNA replication were activated in the high-risk group, indicating abnormal proliferation.

The signature we screened was DRG-related lncRNAs. Therefore, we further assessed the differences in the activation of eight main DDR-related pathways and five radiation-related pathways between the low- and high-risk groups using ssGSEA. Almost all pathways had higher scores in the high-risk group (Fig. 6C).

3.7. Immunity analysis of UCEC samples stratified by the risk signature

We further investigated the relationship between DDR-related signature and UCEC immune microenvironment. As shown, most immune-related pathways were less enriched in the high-risk group (Fig. 6D). Then, we determined the landscape of 28 immune cell infiltrations using ssGSEA. Most immune cells were highly abundant in the low-risk group (Fig. 6E). The stromal, immune, and ESTIMATE scores were significantly low in the high-risk group ($P < 0.05$; Fig. 6F), indicating weak immunity and high tumor purity. Taken together, the poor prognosis in the high-risk group may partly originate from impaired immune function.

Additionally, we compared the levels of the different checkpoints between the two risk subgroups. Most immune checkpoint genes were expressed at low levels in the high-risk group (Fig. 7A). Further analysis revealed that the expression of two most well-known checkpoints, PD1 and CTLA4, were significantly negatively correlated with the risk score (Fig. 7B, E). We also demonstrated that low PD1 (Fig. 7C) or CTLA 4 (Fig. 7F) expression predicted short OS in patients with UCEC. When combining the risk score with PD1 or CTLA4 expression, patients in the high-risk and low-PD1 or high-risk and low-CTLA4 subgroups had the worst prognoses (Fig. 7D, G). Moreover, both IPS (Fig. 7H) and TIDE (Fig. 7I) algorithms suggested that individuals in the high-risk group exhibited poor therapeutic responses to ICB.

3.8. UCEC mutations and chemotherapeutic sensitivity in the DEDRL signature

First, an overview of the top 10 most frequently mutated genes in these two UCEC risk groups was depicted using Oncoplots (Fig. 8A, B). *TP53* (56%) and *PTEN* (85%) had the highest mutation frequencies in the high- and low-risk groups. We also compared the mutation landscapes of the five main DDR-related pathways between the two groups (Fig. S6A–E). Compared to the low-risk group, the high-risk group had lower frequencies of homologous recombination (HR) (27.00% vs. 35.94%, $P = 0.033$) and mismatch repair (MMR) (23.21% vs. 31.25%, $P = 0.045$) mutations (Fig. S6F). In addition, we assessed the MSI status of the patients with UCEC. A higher proportion of patients with MSI was observed in the low-risk group (34.8% vs. 30.2%; Fig. 8C). The MMR-related genes were consistently upregulated in the high-risk group (Fig. S7). In the TCGA-UCEC cohort, the MSI group showed better clinical outcomes (Fig. 8D). Patients with MSI tended to have low risk scores (Fig. 8E). When the tumor samples were separated into four subgroups based on the risk score and microsatellite status, individuals in the high-risk and MSS groups showed the shortest OS (Fig. 8F). TMB is another important parameter that can be used to predict

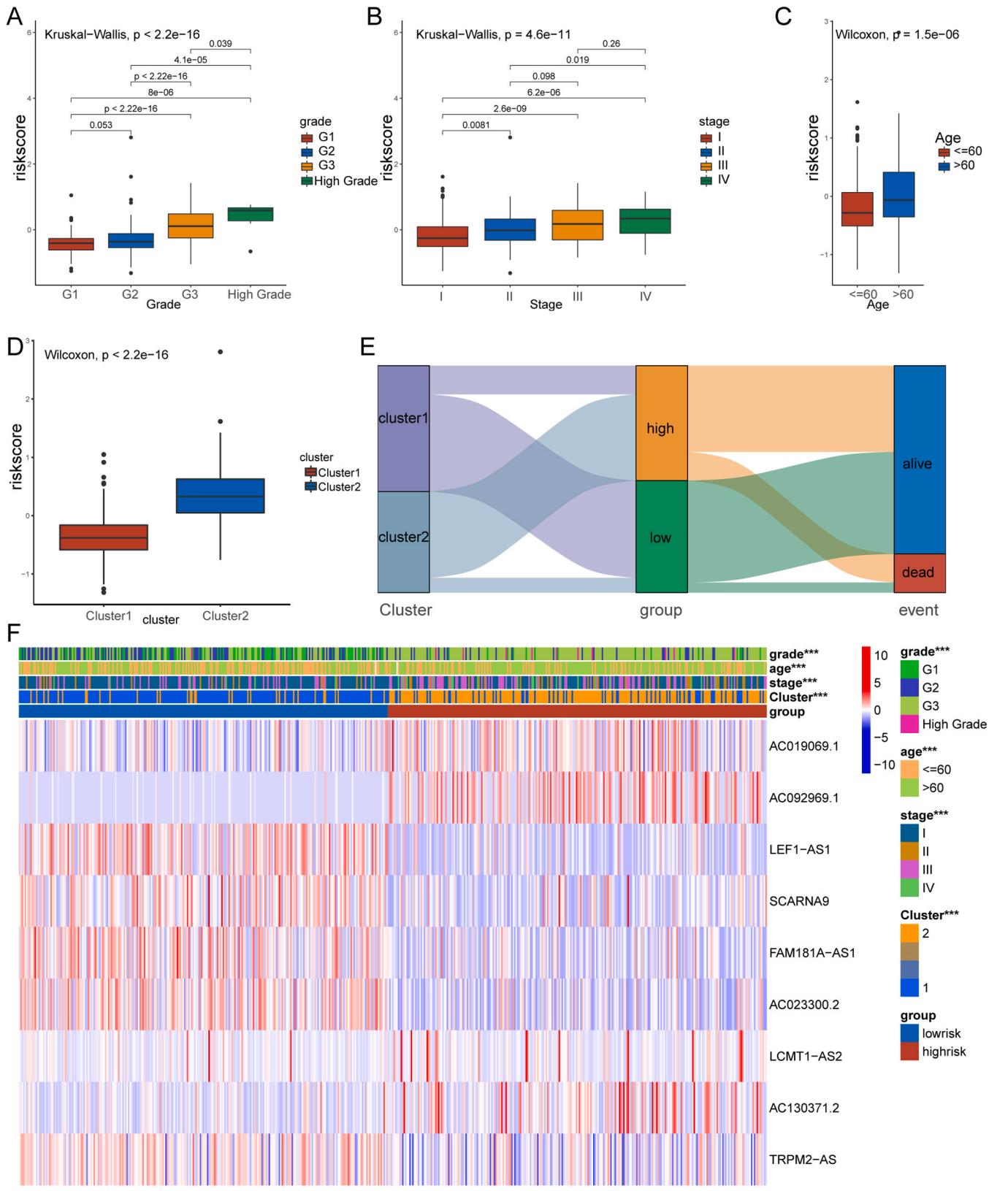

Fig. 4. Relationship between the risk score and different clinicopathological features in the TCGA-UCEC cohort. (A-D) The risk scores in different subgroups stratified by grade (A), stage (B), age (C), and cluster (D). (E) The Sankey diagram depicting the connection among clusters, risk subgroups and survival status. A high proportion of patients in the cluster1 belonged to the low-risk group, and a low proportion of patients in the low-risk group died during the follow-up period. (F) Heatmap showing the correlation between different clinical features and the risk subgroups.

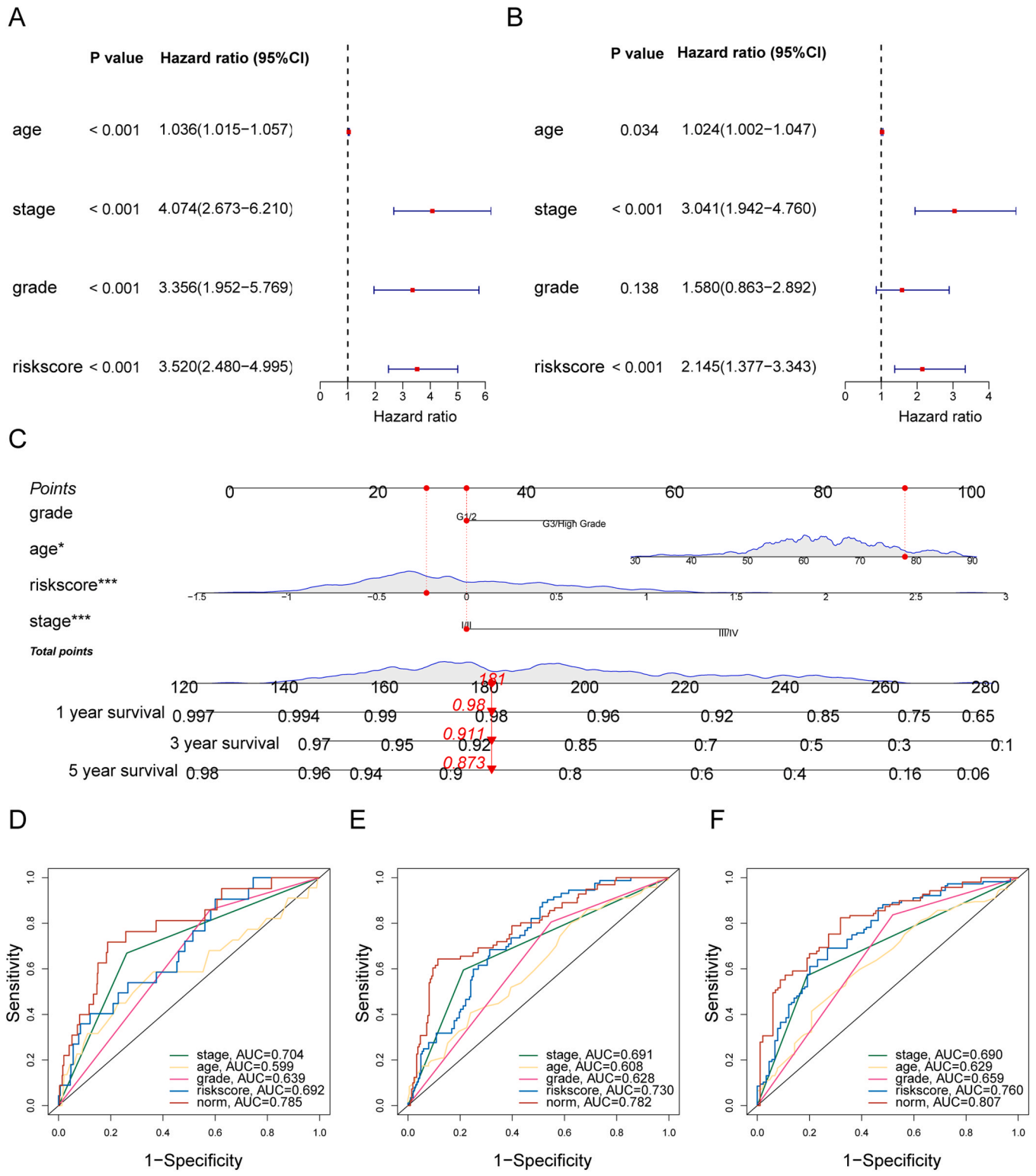

Fig. 5. Construction of a prognostic nomogram for the entire TCGA-UCEC cohort. (A) Univariate Cox regression analysis for the risk score and clinical features. (B) Multivariate Cox regression analysis for the risk score and clinical features. (C) Prognostic nomogram model containing grade, stage, age and risk score. (D-F) Time-dependent ROC analyzes comparing the prognostic accuracy of the risk score and other clinical prognostic features at 1- (D), 3- (E), and 5-year (F) survival time, respectively.

immunotherapeutic responses. The KM curve revealed that high TMB protected against UCEC prognosis (Fig. 8G). We also found that the TMB levels and risk scores were negatively correlated ($P < 0.001$; Fig. 8H). As expected, the high-risk and low-TMB patients showed the worst outcomes (Fig. 8I). Based on the molecular characteristics, immune activity, and mutation heterogeneity of the high-risk group, we reasonably assumed that participants in the high-risk group were prone to acquiring drug resistance. Thus, we comprehensively compared the estimated IC50 of 198 chemotherapeutic agents or inhibitors in GDSC database between the two risk groups. Among these, the IC50 of 26 drugs were

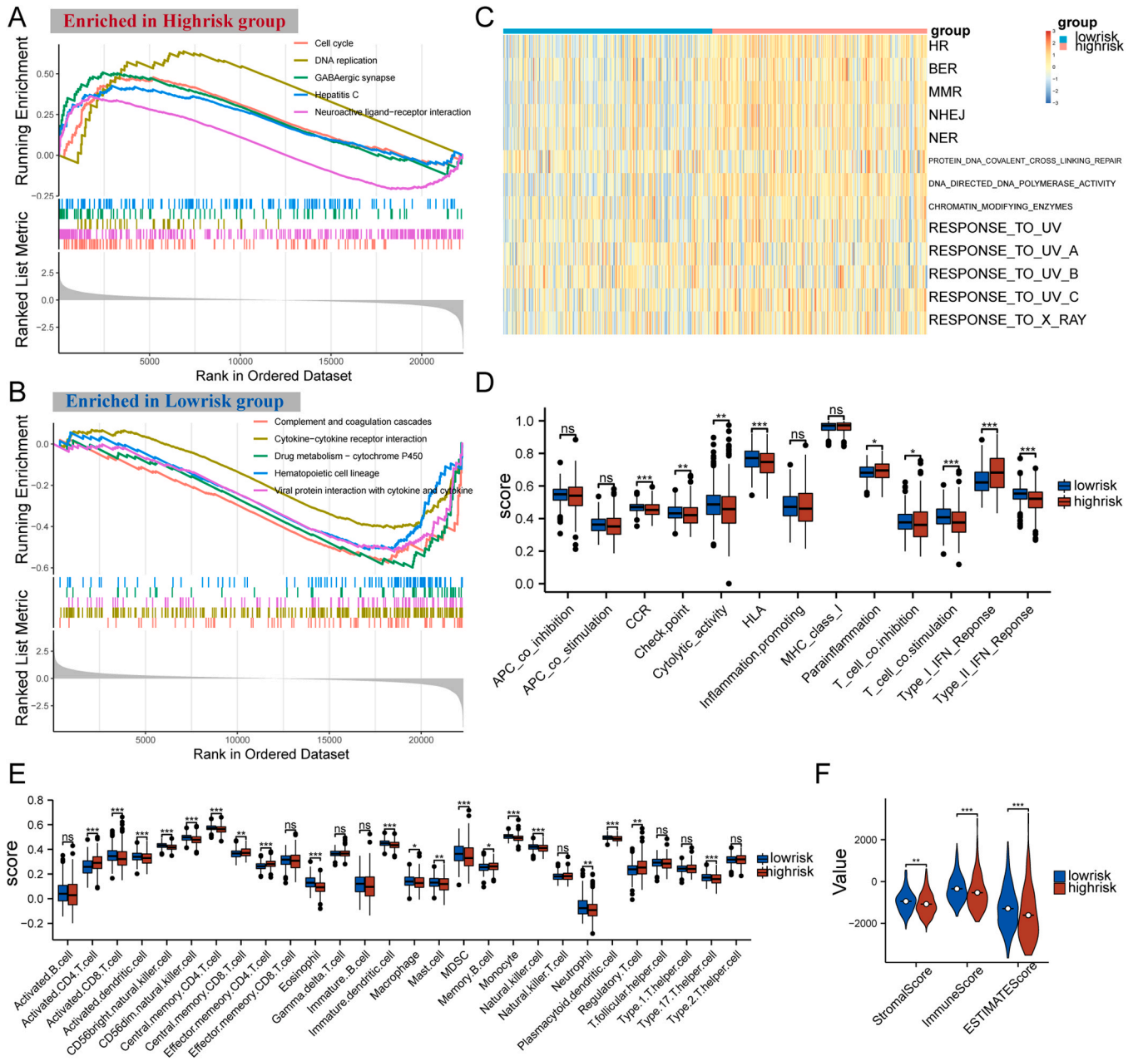

Fig. 6. Functional enrichment and immune characteristics of DEDRL-related signature in UCEC. (A) GSEA analysis of KEGG pathways in high-risk group. (B) GSEA analysis of KEGG pathways in low-risk group. (C) The relative activities of 8 DDR-related pathways and 5 radiation-related pathways calculated by ssGSEA algorithm between low- and high-risk groups. HR, homologous recombination; NHEJ, non-homologous end joining; MMR, mismatch repair; NER, nucleotide excision repair; BER, base excision repair. (D) The boxplot for comparison of 13 immune-related pathways between low- and high-risk groups. CCR, cytokine–cytokine receptor. (E) The abundance of 28 immune cells using ssGSEA algorithm between low- and high-risk groups. (F) The stroma, immune, and ESTIMATE scores between low- and high-risk groups. *p < 0.05, * *p < 0.01, * **p < 0.001, ns, not significant.

significantly different and positively correlated with the risk score (Fig. 8J), indicating that the high-risk UCEC subgroup was potentially insensitive to chemotherapy. Additionally, considering the differences in the mutations of NHEJ- (though not statistically significant), MMR-, HR-related genes between the low-risk and high-risk groups, we further analyzed whether the mutations of these genes would affect the sensitivity of these 26 drugs. As shown in Fig. S8-14, the mutation of these genes could potentially affect the sensitivity to some of the drugs. In most cases, the wild-type of a gene had a higher IC50 than the mutant type did, representing a potential drug resistance.

3.9. AC019069.1 overexpression promoted proliferation and inhibited apoptosis in EC cell lines

To further assess the model robustness, we measured the transcriptional levels of nine signature lncRNAs in 19 paired clinical UCEC specimens. The results showed that AC019069.1, SCARNA9, and TRPM2-AS were upregulated in tumor specimens, whereas LCMT1-AS2, AC130371.2 were downregulated in tumor samples, which was consistent with the findings from TCGA. However, the validation results for AC092969.1, and LEF1-AS1 were contrary to the TCGA data. FAM181A-AS1 and AC023300.2 expression levels did not differ between tumor and normal tissues in our paired samples (Fig. 9A and S15). Among the three verified overexpressed genes, only AC019069.1 indicated a worse

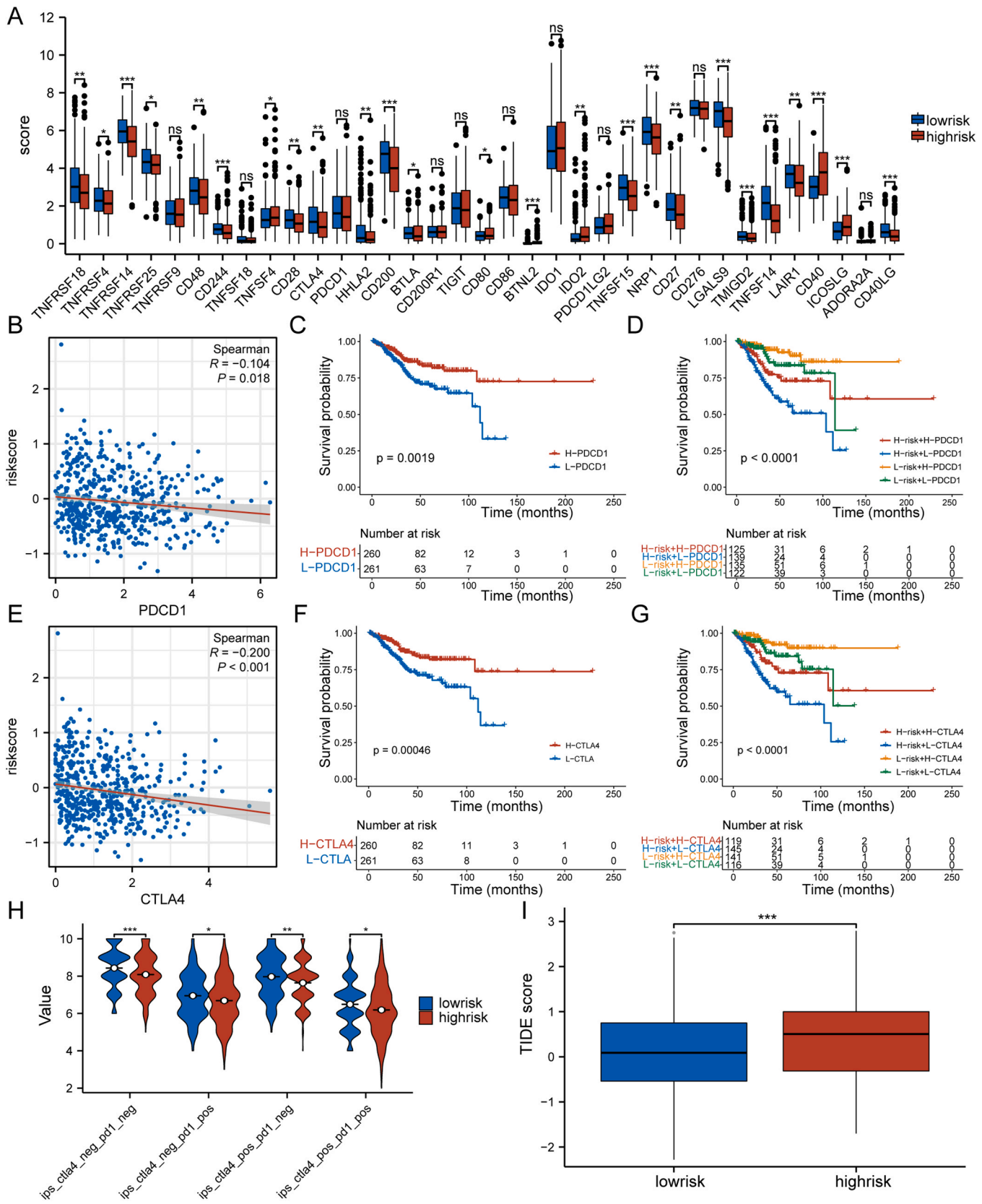

Fig. 7. Comparison of immune checkpoint blockade (ICB) efficacy between low- and high-risk groups. (A) The expression of 35 validated immune checkpoints in these two risk groups. (B, E) The correlation between PD1 (B) or CTLA (E) expression and risk score. (C, F) Kaplan-Meier analyses for PD1 (C) and CTLA4 (F) in UCEC patients. (D, G) Kaplan-Meier analyses in UCEC patients stratified by the expression of PD-1 (D) or CTLA-4 (G) and risk signature. (H) The IPS scores between low- and high-risk groups. (I) The TIDE scores between low- and high-risk groups.

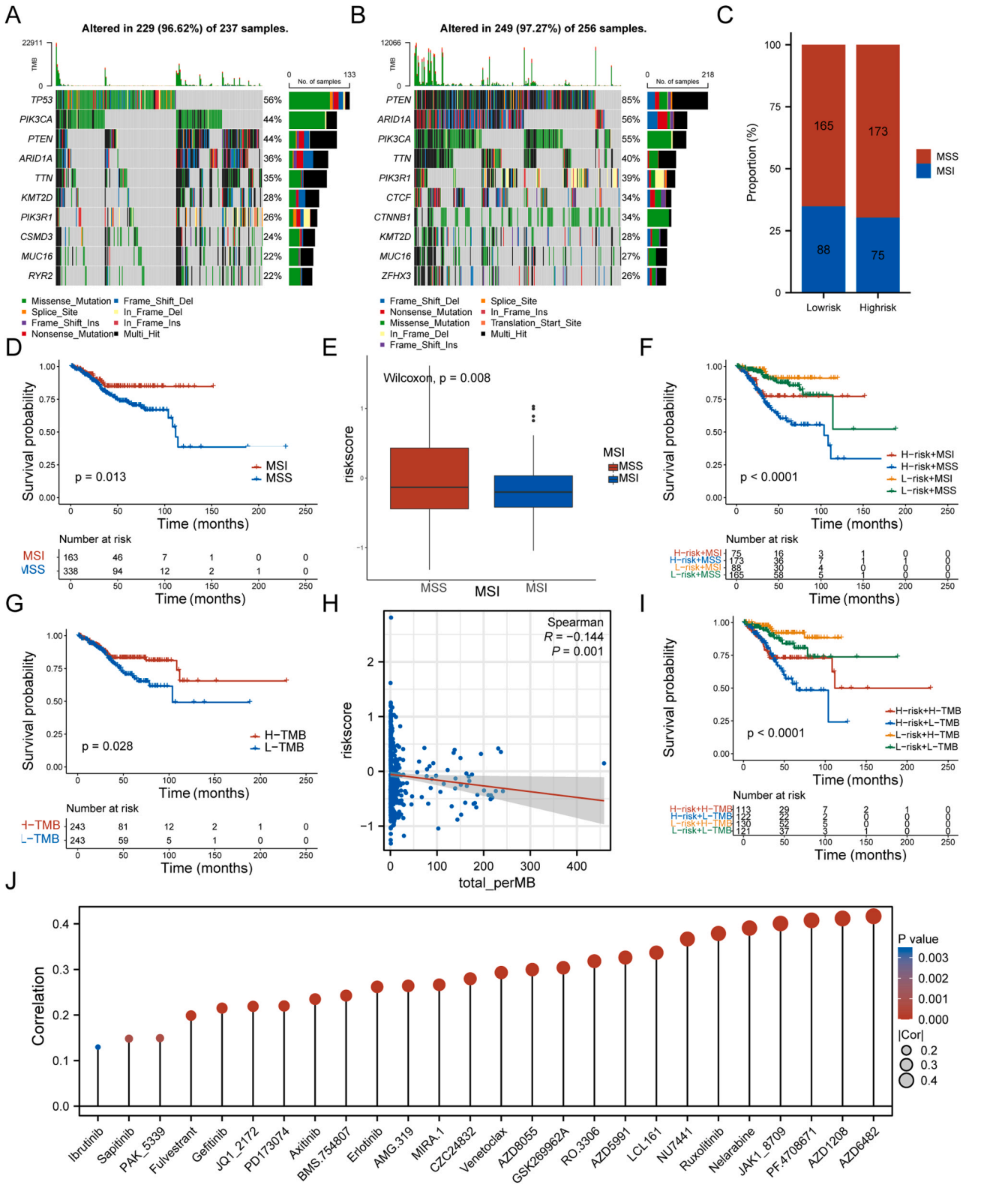

Fig. 8. Mutation profiles and drug sensitivity analyzes based on the DEDRL signature. (A, B) Oncoplots depicting the top ten genes with the highest mutation frequency in high-risk group (A) and low-risk group (B), respectively. (C) Comparison of the proportion of microsatellite status between the low- and the high-risk groups. MSS, microsatellite stability, MSI, microsatellite instability. (D) Kaplan-Meier analyses for microsatellite status in UCEC patients. (E) Comparison of risk scores between MSS and MSI subgroups. (F) Kaplan-Meier analysis in UCEC patients stratified by microsatellite status and risk signature. (G) Kaplan-Meier analyses for tumor mutation burden (TMB) in UCEC patients. (H) The correlation between TMB level and risk score in UCEC patients. (I) Kaplan-Meier analysis in UCEC patients stratified by TMB and risk signature. (J) The correlation analysis for the IC50 of 26 chemicals in GDSC database and risk score. Spearman correlation analysis was applied.

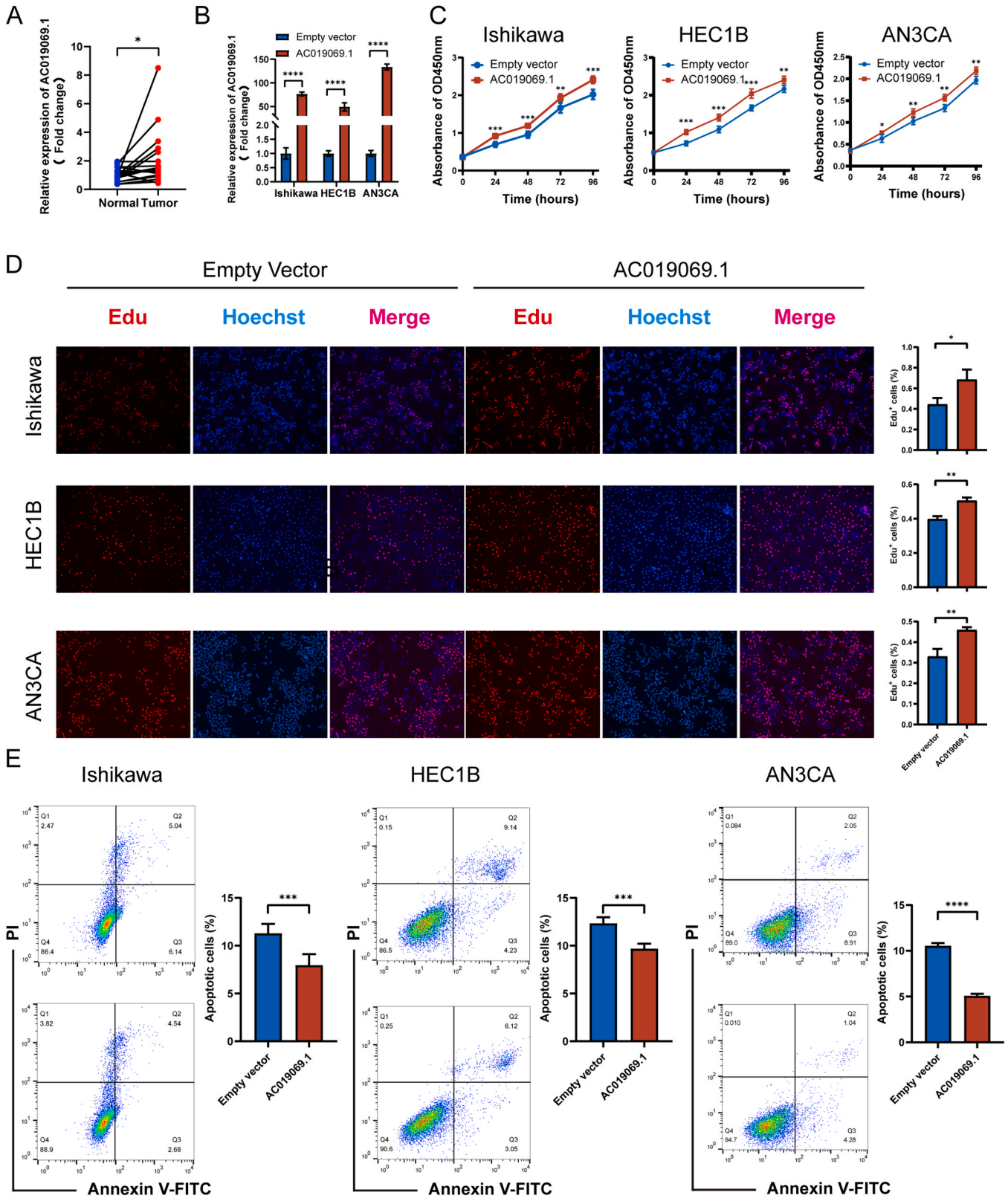

Fig. 9. Functions of AC019069.1 in UCEC. (A) The RNA expression levels of AC019069.1 in 19 paired clinical UCEC samples. (B) qRT-PCR results revealed AC019069.1 was successfully overexpressed in all three EC cell lines. (C) CCK-8 assay revealed AC019069.1-overexpression EC cells proliferated faster. (D) Edu assay revealed AC019069.1-overexpression EC cells proliferated faster. (E) Flow cytometry revealed AC019069.1-overexpression EC cells had lower apoptosis rates. *p < 0.05, * *p < 0.01, * **p < 0.001, * ** *p < 0.0001.

prognosis; therefore, we further explored its potential function.

To assess the potential function of AC019069.1 in UCEC, we conducted a series of in vitro experiments. Firstly, AC019069.1 was demonstrated to be successfully overexpressed in three EC cell lines (Fig. 9B). Additionally, CCK-8 and EdU assays revealed that AC019069.1 accelerated the growth of Ishikawa, HEC1B, and ANC3A cells (Fig. 9C, D). Moreover, AC019069.1-overexpressing EC cells exhibited significantly low apoptosis rates (Fig. 9E).

3.10. AC019069.1 protected EC cells from etoposide-induced DNA damage stimuli

As previously mentioned, the high-risk group exhibited proficient DDR ability; therefore, we wondered whether AC019069.1 was involved in DDR. In the TCGA-UCEC dataset, AC019069.1 was correlated with most of the DDR regulators (Fig. 10A). Moreover, all five classical DDR pathways had higher activities in the high-AC019069.1 group (Fig. 10B). To further explore its involvement in EC, we treated EC cell lines with etoposide to induce DNA damage. We first determined that etoposide at 20 μM could induce significant DNA damage in all three EC cell lines (Fig. S16A), while significant damage recovery could be observed at 4 h after drug withdrawal (Fig. S16B). DNA damage stimuli elicited the upregulation of AC019069.1, indicating that AC019069.1 was responsive to DNA damage (Fig. 10C). In addition, we monitored DDR in UCEC by detecting the γ-H2AX changes. The immunofluorescence assay revealed that AC019069.1 overexpression did not alter baseline genome stability, whereas AC019069.1-overexpressing EC cells exhibited decreased levels of DNA damage after etoposide treatment compared to controls (Fig. 10D). Western blot analysis also verified the role of AC019069.1 in maintaining genome stability, as AC019069.1 overexpression protected EC cells from etoposide-induced DNA damage stimuli and conferred quick recovery from DNA damage (Fig. 10E, F).

4. Discussion

DDR counteracted tumorigenesis by maintaining genomic integrity. However, cancer cells could also use this system to develop resistance to radiotherapy and many chemotherapeutic drugs [22]. Till date, targeting DDR pathways remains a promising strategy for sensitizing cancer therapies, especially in DDR-proficient tumors. In this study, we found that DDR was significantly enriched in UCEC. A previous study has successfully established a nine DDR mRNA-based classifier for predicting UCEC prognosis [23]. Considering that lncRNAs are pivotal in UCEC progression, linking DDR signaling with lncRNA regulators may provide novel insights into the improvement of clinical management of UCEC.

Compelling evidence reveals the intrinsic heterogeneity of UCEC. In this study, 204 DEDRLs were identified. Based on the expression profile of these lncRNAs, two distinctive UCEC clusters were identified. Comprehensive analyses indicated that the prognosis, TME, and immunoreactivity of these subtypes were significantly different. In summary, our results provide consensus that precise molecular classification has practical and clinical significance.

However, poor accessibility of transcriptome profiles to patients in clinical practice may limit the application of DEDRLs. Therefore, a concise but optimal 9-DEDRL based risk signature was identified using Cox and LASSO regression. The risk score exhibited promising value in predicting prognosis and guiding precise individual therapies for UCEC. And we successfully constructed a nomogram by integrating risk score, age, grade, and stage to guide clinical practice. In fact, age, stage, and grade are all important factors affecting DDR. Age could affect DDR efficiency, and DDR efficiency also contributes to the occurrence and progression of age-related diseases, such as cancer[24]. Lantuejoul et al. reported that during lung carcinogenesis, the expression of DDR-related proteins significantly correlated with tumor stage and grade [25], which highlights the impact of tumor grade and stage on DDR. Additionally, the risk signature was closely associated with immune cell infiltration, ICB efficacy, TMB, MSI, and chemosensitivity. We further analyzed the mechanisms underlying the different characteristics of the low- and high-risk groups. GSEA indicated that two important cancer hallmarks, cell cycle [26] and DNA replication [27], were enriched in the high-risk group. These molecular features may confer aggressive phenotypes to cancer cells, resulting in poor clinical outcomes. More importantly, GSEA revealed that the high-risk group had a high activity of pathways related to DDR, X-ray, and UV responses. These results indicate potential chemoradiotherapy resistance in the high-risk group owing to a proficient DDR system. Consistently, we found that subjects in the high-risk group were less sensitive to common drugs or inhibitors in the GDSC database.

The human body has powerful immune surveillance capabilities to eliminate cancer cells [28]. However, to overcome this barrier, tumor cells have evolved a series of mechanisms based on the tumor microenvironment, a tumorigenic primary niche suitable for tumor progression [29]. In this study, we found low infiltration of most immune cell types and weak activity of most immune-related pathways in the DDR-proficient high-risk group, representing a “cold immunity” status. In addition, most checkpoint molecules, including PD1 (although not statistically significant) and CTLA4, were also downregulated in the high-risk group, indicating that individuals in this group may hardly benefit from ICB therapy, and results from IPS and TIDE analyses confirmed this assumption. Surprisingly, several studies have revealed that DDR-targeted therapies have efficient antitumor capabilities [22,30]. Briefly, targeting DDR elicits a DNA damage-induced immune response to eradicate cancer cells. Considering the potential resistance to chemoradiotherapy and immunotherapy, DDR inhibitors may be used to improve the outcomes of patients classified as high-risk groups.

Previous studies have suggested that TMB is a promising predictor of ICB-based strategies [31,32]. Somatic mutations in cancer cell DNA can produce neoantigens that can be traced and targeted by immune guardians [33,34]. Thus, the TMB level of a tumor is likely to be positively correlated with the neoantigen load. In our study, a significant negative relationship was found between TMB and the risk score. In concordance with previous reports [35], we found that high TMB tended to predict good prognosis in the TCGA-UCEC project. Another argument supporting the selection of high-risk groups for treatment with DDR inhibitors is that such therapies may promote tumor antigenicity by disrupting genomic stability and increasing mutability. In addition, MSI secondary to DNA mismatch repair deficiency (MMR-D) has recently been identified as a valuable biomarker of sensitivity to immunotherapy [36]. The MSI/MMR-D endometrial carcinomas subtype reportedly exhibits good patient survival and immune activity [37]. In TCGA-UCEC dataset, we found that patients with MSI had a longer OS than those with MSS. Moreover, MMR-related genes were mutated less frequently and exhibited high expression levels in the high-risk group. This finding is consistent with the low proportion of patients with MSI in the high-risk group.

Additionally, we confirmed that AC019069.1 might act as an oncogene in EC in vitro. The proliferation rate and apoptotic tendency of AC019069.1-overexpressing cells were high and low, respectively, representing an aggressive phenotype. Till date, no studies have revealed the biological functions of AC019069.1. DNA double strand breaks (DSBs) belong to one of the most lethal types of damage [38] and γ-H2AX is a sensitive marker for this process [39]. Etoposide is commonly used as a DSB inducer [40,41], and in mammalian cells, DSBs are usually repaired by HR and NHEJ pathways [42]. In the TCGA-UCEC dataset, the relative activities of HR and NHEJ were significantly different between low-AC019069.1 and high-AC019069.1 groups. Consistently, in this study, AC019069.1 overexpression could contribute to the resistance of EC cells to etoposide-induced DNA damage, which might be a possible mechanism underlying its carcinogenic effect.

Nevertheless, some limitations exist in our study. First, although we verified the expression levels of signature lncRNAs in our samples but did not further validate the prognostic value of the risk score because of

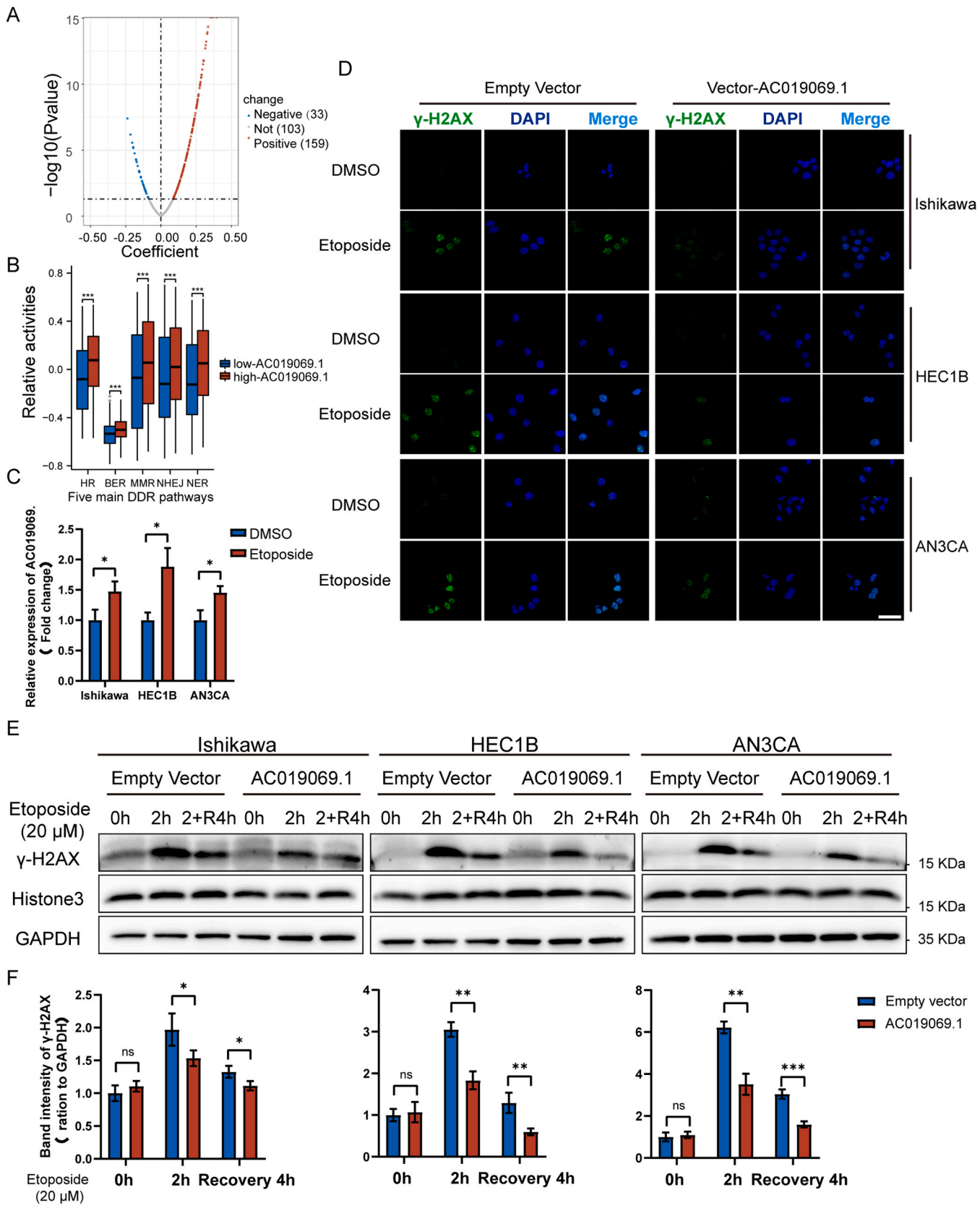

Fig. 10. AC019069.1 overexpression stabilized EC cell genome. (A) The volcano plot depicting the correlation between AC019069.1 and DDR genes. (B) The ssGSEA scores of five classical DDR pathways between low- and high-AC019069.1 TCGA-UCEC subgroups. (C) The RNA levels of AC019069.1 in EC cell lines after etoposide (20 μM) treatment for 24 h. (D) Immunofluorescence results suggested that AC019069.1-overexpressing EC cells were resistant to etoposide induced DNA damage. The EC cells were treated with DMSO or etoposide (20 μM) for 2 h. (E) Western blot analysis suggested that AC019069.1-overexpressing EC cells showed decreased DNA damage and recovered more quickly. The EC cells were treated with etoposide (20 μM) for 2 h to induce DNA damage or allowed to recover for 4 h. (F) The statistical analysis of western blot results. *$p < 0.05$, * *$p < 0.01$, * **$p < 0.001$, ns, not significant.

the lack of patient follow-up data. Second, the specific mechanism of AC019069.1-regulated DDR in UCEC has not been elucidated. Third, the biological functions of the remaining eight signature lncRNAs in UCEC remain unclear and require further verification.

5. Conclusion

In summary, we successfully constructed a nine DRL-based robust risk signature that showed potential value for predicting UCEC prognosis. Additionally, comprehensive bioinformatics analyses revealed that the high-risk patients with UCEC were DDR-proficient, immune surveillance impaired, and potentially drug-resistant, and thus had worse clinical outcomes. Our findings shed new light on precise UCEC management.

CRediT authorship contribution statement

Tao Wang: Conceptualization, Methodology, Software, Visualization, Validation and Writing – original draft. **Mei Ji:** Visualization, Validation. **Wenwen Liu:** Validation. **Jing Sun:** Conceptualization, Supervision, Writing – review & editing. All authors contributed to manuscript revision, read, and approved the submitted version.

Declaration of Competing Interest

None declared.

Acknowledgments

This work was supported by grants from the Science and Technology Commission of Shanghai Municipality (22Y11906100) to Jing Sun and Shanghai Outstanding Academic Leaders Plan to Jing Sun (Year 2019).

Human and animal rights

The research protocol was approved by the Medical Ethics Committee of Shanghai First Maternity and Infant Hospital (KS22356). All procedures were performed strictly in compliance with the Declaration of Helsinki 1964 or equivalent ethical principles. And written informed consent was acquired from all subjects.

Appendix A. Supporting information

Supplementary data associated with this article can be found in the online version at doi:10.1016/j.csbj.2023.10.025.

References

[1] Cronin KA, et al. Annual report to the nation on the status of cancer, part 1: national cancer statistics. Cancer 2022;128(24):4251–84.
[2] Siegel RL, et al. Cancer statistics, 2022. CA Cancer J Clin 2022;72(1):7–33.
[3] Amant F, et al. Endometrial cancer. Lancet 2005;366(9484):491–505.
[4] Jeggo PA, Pearl LH, Carr AM. DNA repair, genome stability and cancer: a historical perspective. Nat Rev Cancer 2016;16(1):35–42.
[5] O'Connor MJ. Targeting the DNA damage response in cancer. Mol Cell 2015;60(4):547–60.
[6] Zheng C, et al. FANCD2 promotes the malignant behavior of endometrial cancer cells and its prognostic value. Exp Cell Res 2022;421(2):113388.
[7] Takeuchi M, et al. Anti-tumor effect of inhibition of DNA damage response proteins, ATM and ATR, in endometrial cancer cells. Cancers 2019;11(12).
[8] Esposito R, et al. Hacking the cancer genome: profiling therapeutically actionable long non-coding RNAs using CRISPR-Cas9 screening. Cancer Cell 2019;35(4):545–57.
[9] Tan YT, et al. LncRNA-mediated posttranslational modifications and reprogramming of energy metabolism in cancer. Cancer Commun (Lond) 2021;41(2):109–20.
[10] Liu H, Wan J, Chu J. Long non-coding RNAs and endometrial cancer. Biomed Pharm 2019;119:109396.
[11] He WP, et al. A novel necroptosis-related lncRNA signature for predicting prognosis and anti-cancer treatment response in endometrial cancer. Front Immunol 2022;13:1018544.
[12] Ding H, et al. Prediction of clinical outcome in endometrial carcinoma based on a 3-lncRNA signature. Front Cell Dev Biol 2021;9:814456.
[13] Jiang Y, et al. Construction of a Glycolysis-related long noncoding RNA signature for predicting survival in endometrial cancer. J Cancer 2021;12(5):1431–44.
[14] Li Q, et al. The DDR-related gene signature with cell cycle checkpoint function predicts prognosis, immune activity, and chemoradiotherapy response in lung adenocarcinoma. Respir Res 2022;23(1):190.
[15] Ritchie ME, et al. limma powers differential expression analyses for RNA-sequencing and microarray studies. Nucleic Acids Res 2015;43(7):e47.
[16] Wilkerson MD, Hayes DN. ConsensusClusterPlus: a class discovery tool with confidence assessments and item tracking. Bioinformatics 2010;26(12):1572–3.
[17] Yoshihara K, et al. Inferring tumour purity and stromal and immune cell admixture from expression data. Nat Commun 2013;4:2612.
[18] Charoentong P, et al. Pan-cancer immunogenomic analyses reveal genotype-immunophenotype relationships and predictors of response to checkpoint blockade. Cell Rep 2017;18(1):248–62.
[19] Jiang P, et al. Signatures of T cell dysfunction and exclusion predict cancer immunotherapy response. Nat Med 2018;24(10):1550–8.
[20] Mayakonda A, et al. Maftools: efficient and comprehensive analysis of somatic variants in cancer. Genome Res 2018;28(11):1747–56.
[21] Hause RJ, et al. Classification and characterization of microsatellite instability across 18 cancer types. Nat Med 2016;22(11):1342–50.
[22] Reisländer T, Groelly FJ, Tarsounas M. DNA damage and cancer immunotherapy: a STING in the tale. Mol Cell 2020;80(1):21–8.
[23] Liu J, et al. Construction of a nine DNA repair-related gene prognostic classifier to predict prognosis in patients with endometrial carcinoma. BMC Cancer 2021;21(1):29.
[24] Reinhardt HC, Schumacher B. The p53 network: cellular and systemic DNA damage responses in aging and cancer. Trends Genet 2012;28(3):128–36.
[25] Lantuejoul S, et al. Telomere maintenance and DNA damage responses during lung carcinogenesis. Clin Cancer Res 2010;16(11):2979–88.
[26] Liu J, Peng Y, Wei W. Cell cycle on the crossroad of tumorigenesis and cancer therapy. Trends Cell Biol 2022;32(1):30–44.
[27] Macheret M, Halazonetis TD. DNA replication stress as a hallmark of cancer. Annu Rev Pathol 2015;10:425–48.
[28] Miao Y, et al. Adaptive immune resistance emerges from tumor-initiating stem cells. Cell 2019;177(5):1172–1186.e14.
[29] Gajewski TF, Schreiber H, Fu YX. Innate and adaptive immune cells in the tumor microenvironment. Nat Immunol 2013;14(10):1014–22.
[30] Chabanon RM, et al. Targeting the DNA damage response in immuno-oncology: developments and opportunities. Nat Rev Cancer 2021;21(11):701–17.
[31] Chan TA, et al. Development of tumor mutation burden as an immunotherapy biomarker: utility for the oncology clinic. Ann Oncol 2019;30(1):44–56.
[32] Samstein RM, et al. Tumor mutational load predicts survival after immunotherapy across multiple cancer types. Nat Genet 2019;51(2):202–6.
[33] Snyder A, et al. Genetic basis for clinical response to CTLA-4 blockade in melanoma. N Engl J Med 2014;371(23):2189–99.
[34] Riaz N, et al. The role of neoantigens in response to immune checkpoint blockade. Int Immunol 2016;28(8):411–9.
[35] Liu J, et al. Development of an oxidative phosphorylation-related and immune microenvironment prognostic signature in uterine corpus endometrial carcinoma. Front Cell Dev Biol 2021;9:753004.
[36] Baretti M, Le DT. DNA mismatch repair in cancer. Pharm Ther 2018;189:45–62.
[37] Guo YE, et al. The clinicopathological characteristics, prognosis and immune microenvironment mapping in MSI-H/MMR-D endometrial carcinomas. Discov Oncol 2022;13(1):12.
[38] You Z, Bailis JM. DNA damage and decisions: CtIP coordinates DNA repair and cell cycle checkpoints. Trends Cell Biol 2010;20(7):402–9.
[39] Bonner WM, et al. GammaH2AX and cancer. Nat Rev Cancer 2008;8(12):957–67.
[40] Montecucco A, Biamonti G. Cellular response to etoposide treatment. Cancer Lett 2007;252(1):9–18.
[41] Tang M, et al. SMYD2 inhibition-mediated hypomethylation of Ku70 contributes to impaired nonhomologous end joining repair and antitumor immunity. Sci Adv 2023;9(24):eade6624.
[42] Shrivastav M, De Haro LP, Nickoloff JA. Regulation of DNA double-strand break repair pathway choice. Cell Res 2008;18(1):134–47.